RBS: Rutherford Backscattering Spectrometry

Valentino Rigato (INFN-LNL)

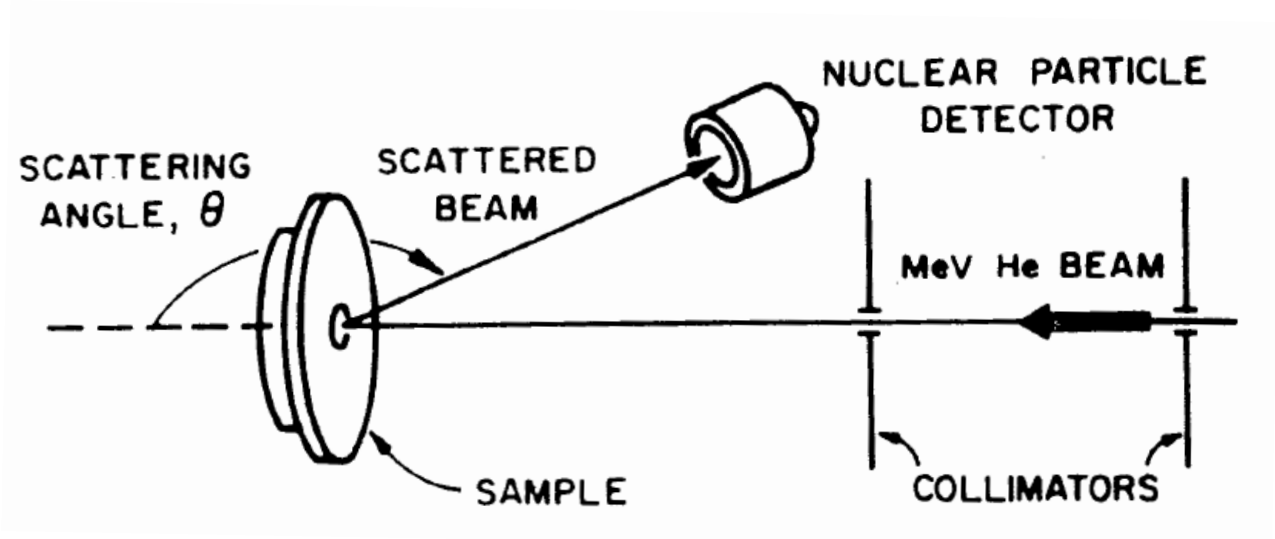

Θ=150°

E_0=2.5 MeV

Schematic of the experimental setup for Rutherford backscattering. A collimated beam of He ions is incident on a planar sample. Particles scattered to an angle θ are detected by a solid state nuclear particle detector. All this apparatus must be under vacuum.

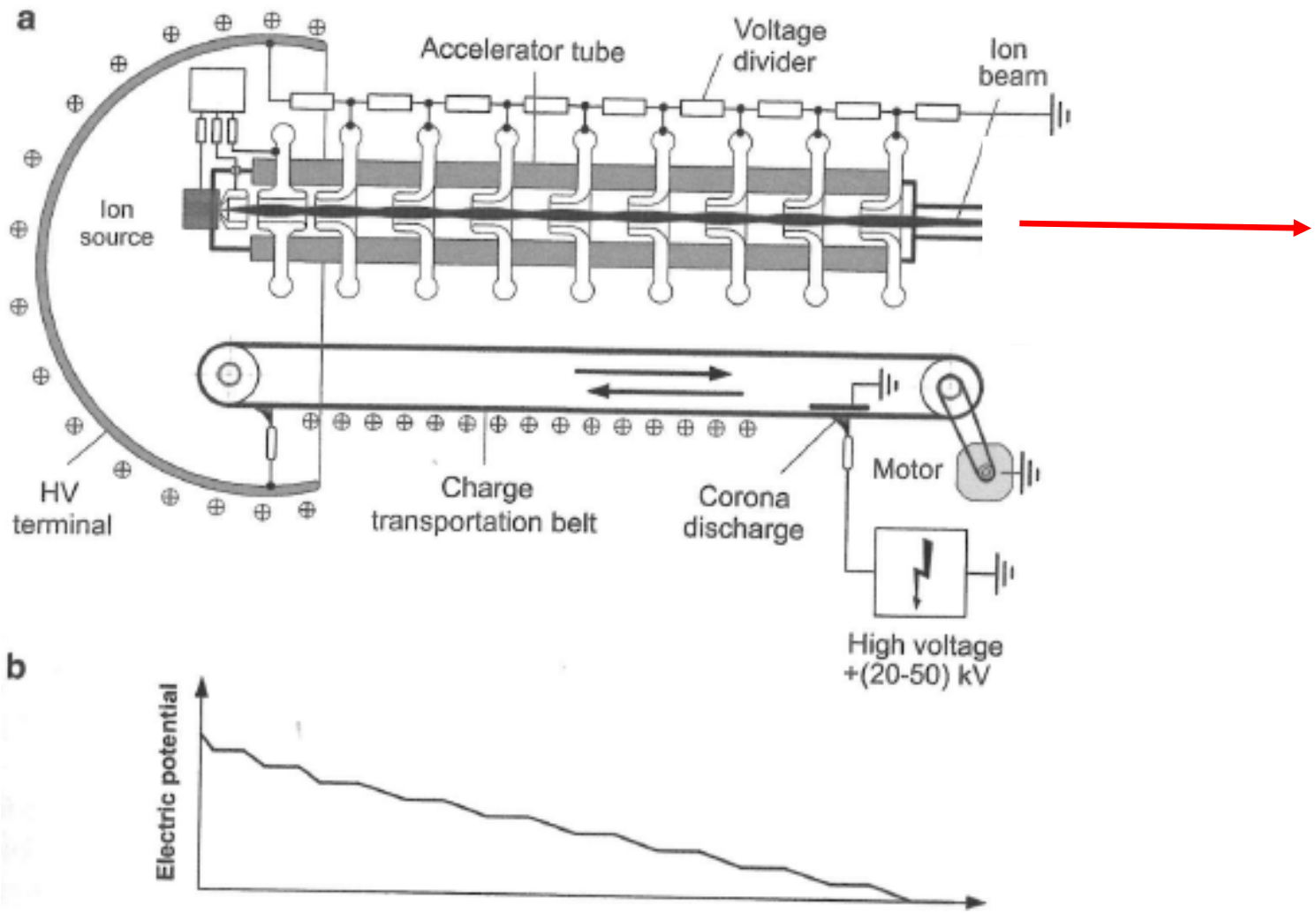

Scheme of the Van de Graaff generator (**a**) and (**b**) the accelerating potential

KINEMATICS OF ELASTIC COLLISION

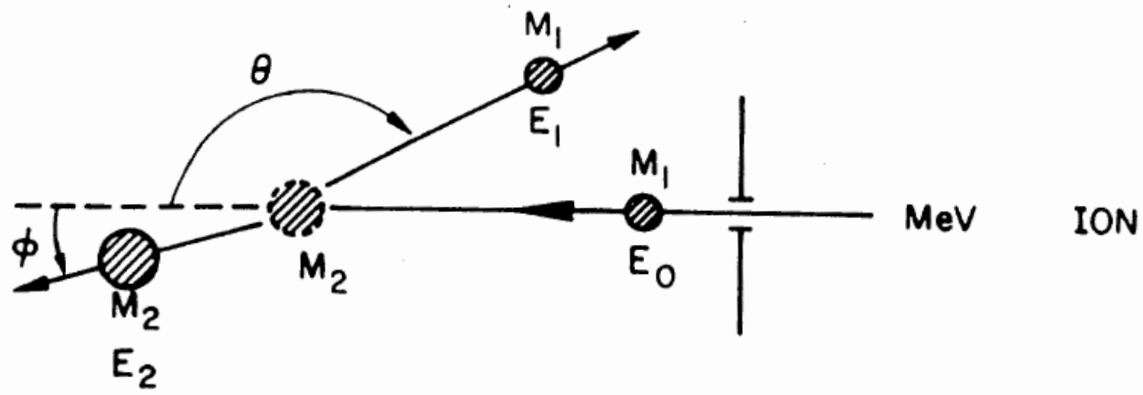

Schematic representation of an elastic collision between a projectile of mass M_1 and energy E_0 and a target mass M_2 which is initially at rest. After the collision, the projectile and target mass have energies E_1 and E_2 respectively. The angles θ and ϕ are positive as shown.

All quantities refer to a laboratory frame of reference.

For $M_1 < M_2$, conservation of energy and momentum, gives:

$$\frac{E_1}{E_0} = \left[\frac{(M_2^2 - M_1^2\sin^2\theta)^{1/2} + M_1\cos\theta}{M_1 + M_2}\right]^2$$

$$E_1 = K_{M_2}E_0$$

K_{M_2} = kinematic factor

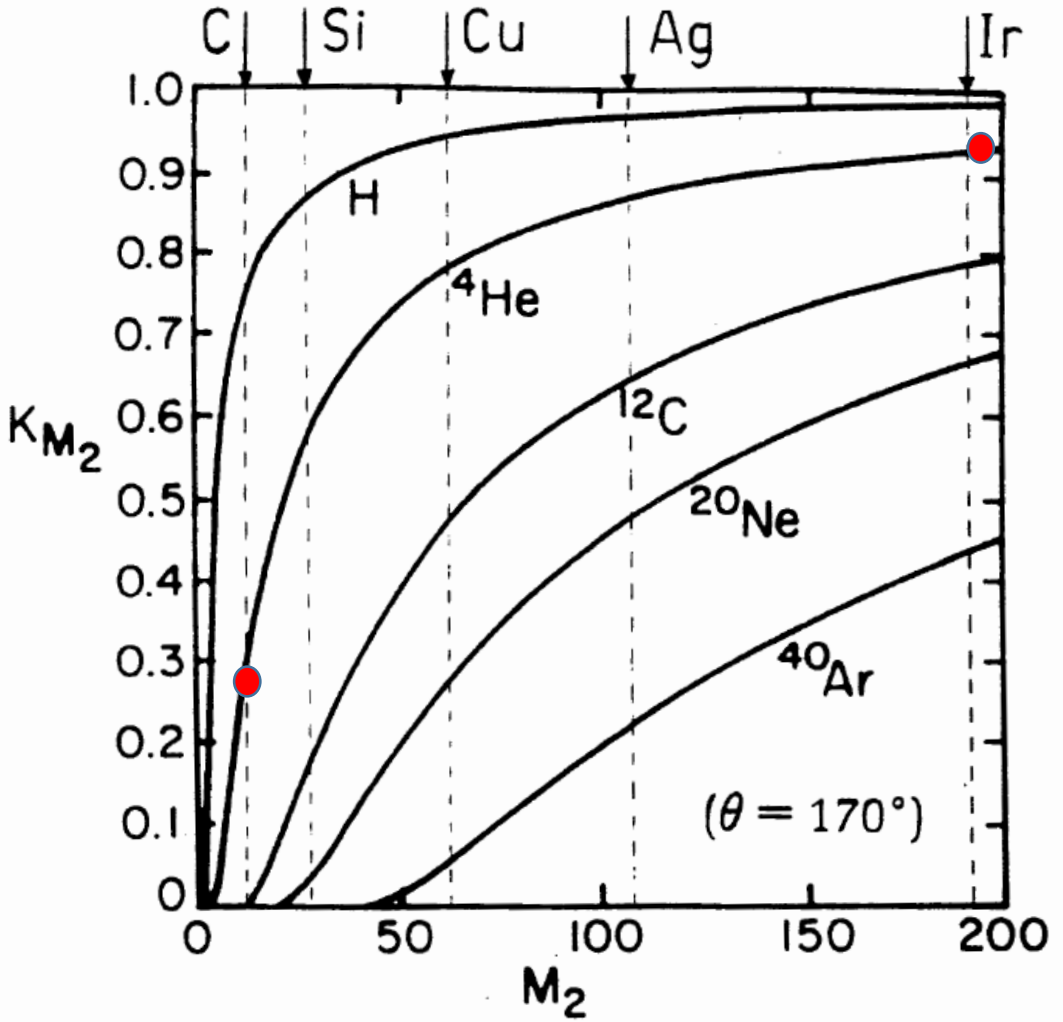

K_{Au}(He,150°)=0.9270

K_C (He,150°)=0.2736

K_O (He,150°)=0.3848

Two different atoms , A and B, with masses M_A and M_B, are distinguished if the energy difference:

$$\Delta E_1 = E_1(M_A) - E_1(M_B) = (K_{M_A} - K_{M_B})E_0$$

is larger than the energy resolution of the whole detecting apparatus (detector + electronics).

ΔE_1 is large when either

E_0 is large
or
$(K_{M_A} - K_{M_B})$ is large.

E_0 is limited only by the maximum operating voltage of the accelerator. Anyhow it must be lower than the threshold for nuclear interactions.

$(K_{M_A} - K_{M_B})$ increases as the scattering angle increases:

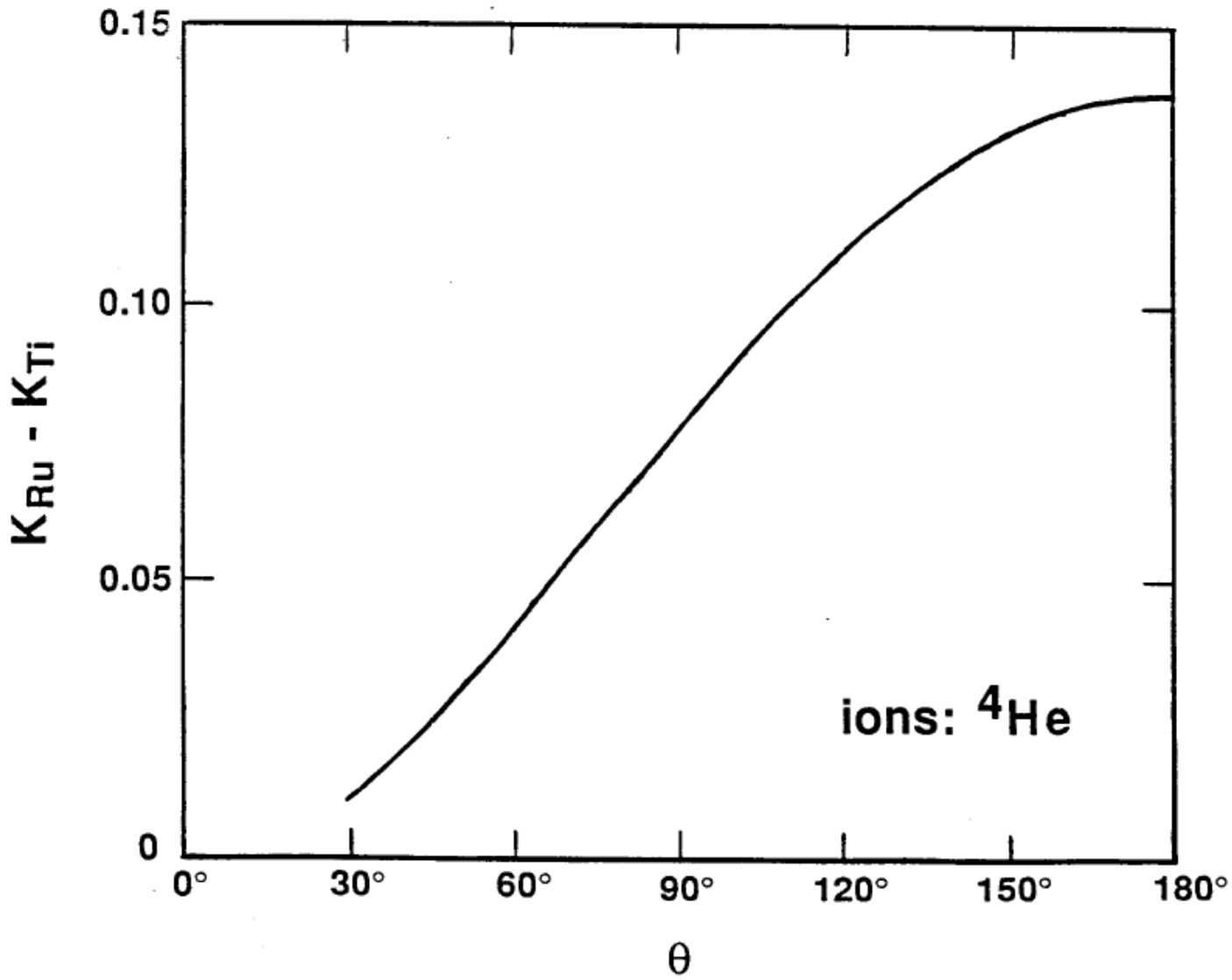

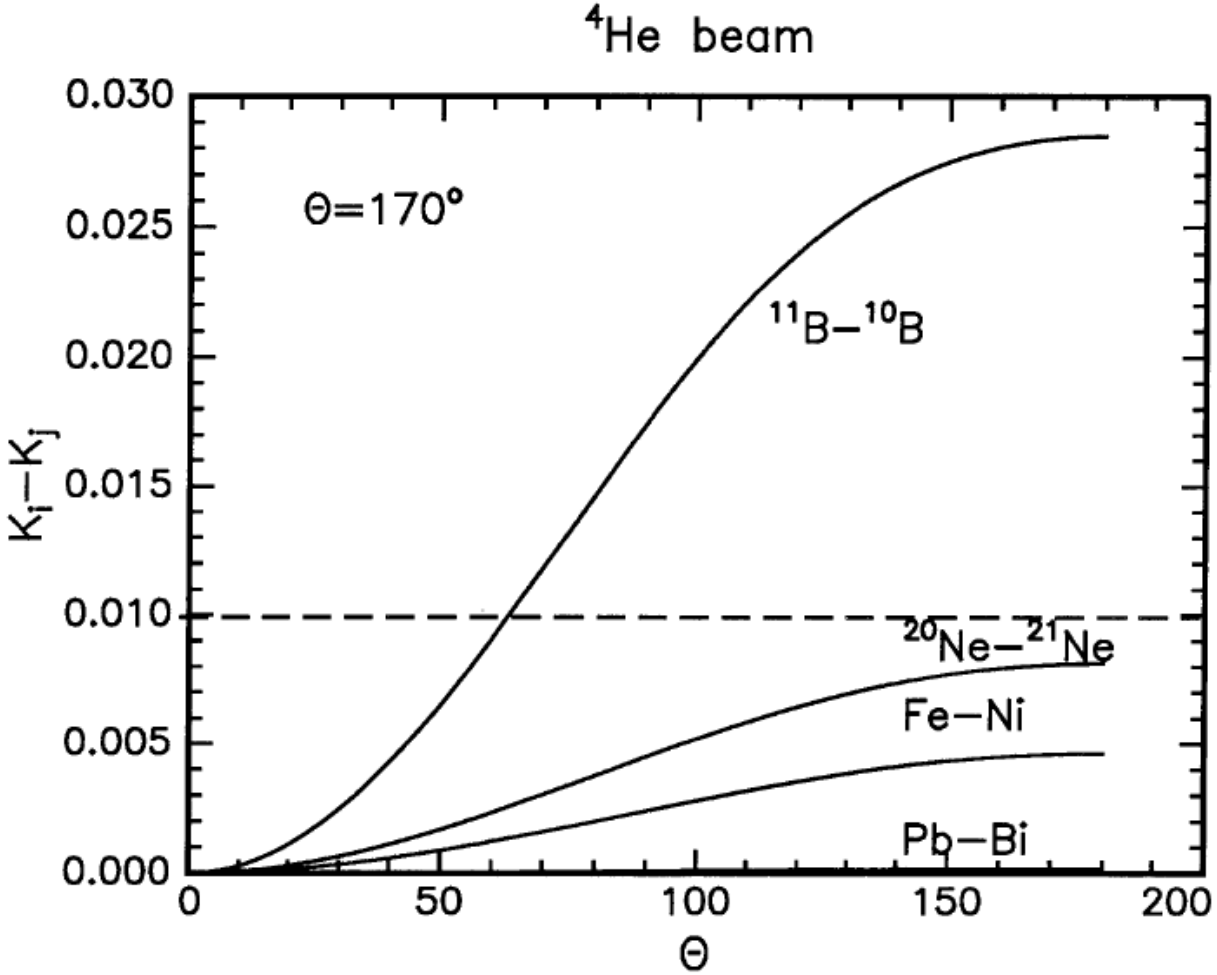
^{4}He beam
Θ=170°
^{11}B–^{10}B
^{20}Ne–^{21}Ne
Fe–Ni
Pb–Bi
$K_i - K_j$
Θ
0.030
0.025
0.020
0.015
0.010
0.005
0.000
0
50
100
150
200

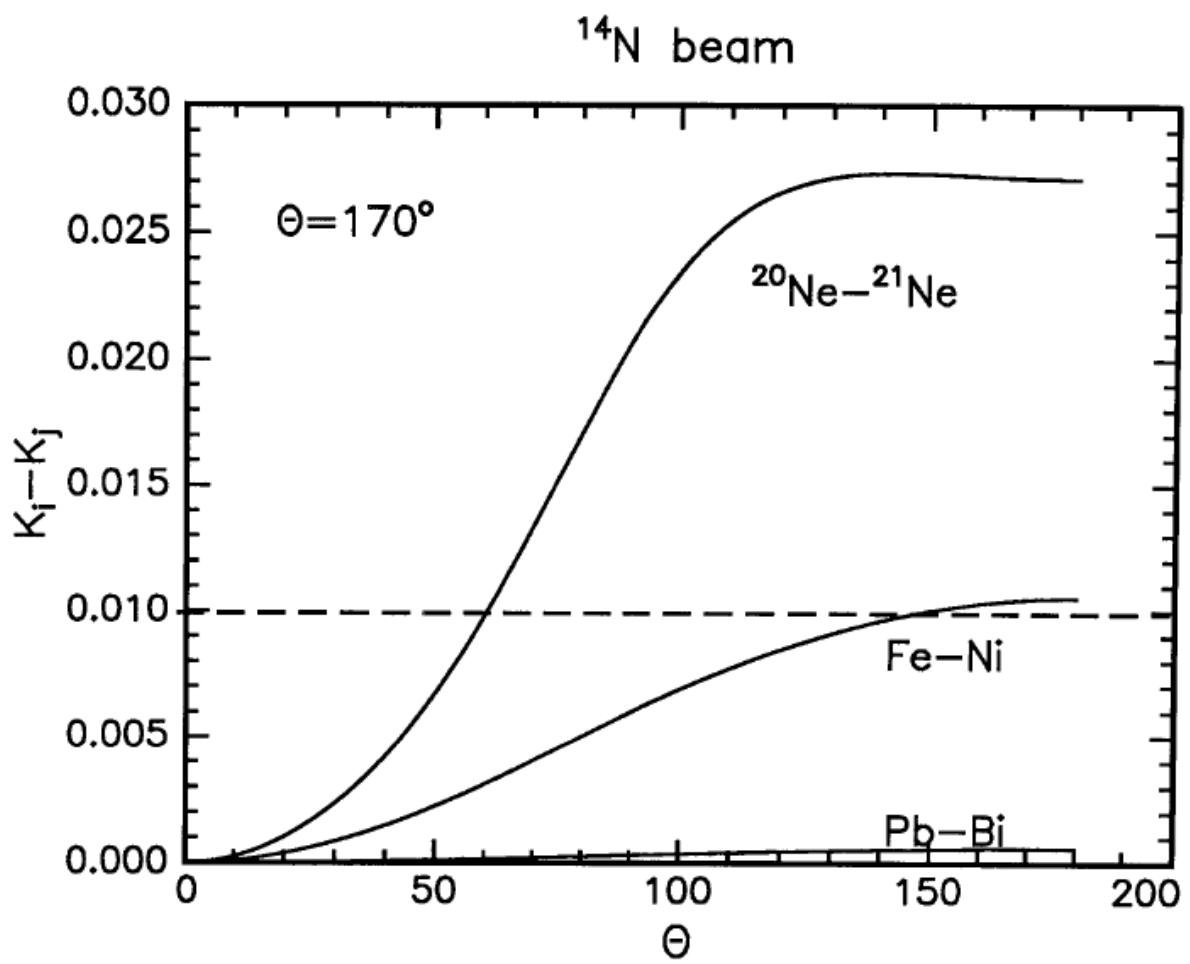
^{14}N beam
Θ=170°
^{20}Ne–^{21}Ne
Fe–Ni
Pb–Bi
$K_i - K_j$
Θ
0.030
0.025
0.020
0.015
0.010
0.005
0.000
0
50
100
150
200

$(K_{M_A} - K_{M_B})$ is a strong function of the mass M_1 of the incident ion:

For distinguishing heavy atoms there might seem some advantage in using heavy ion beams. but...

the energy resolution of the commonly used solid state detector deteriorates even more rapidly with increasing Z_1:

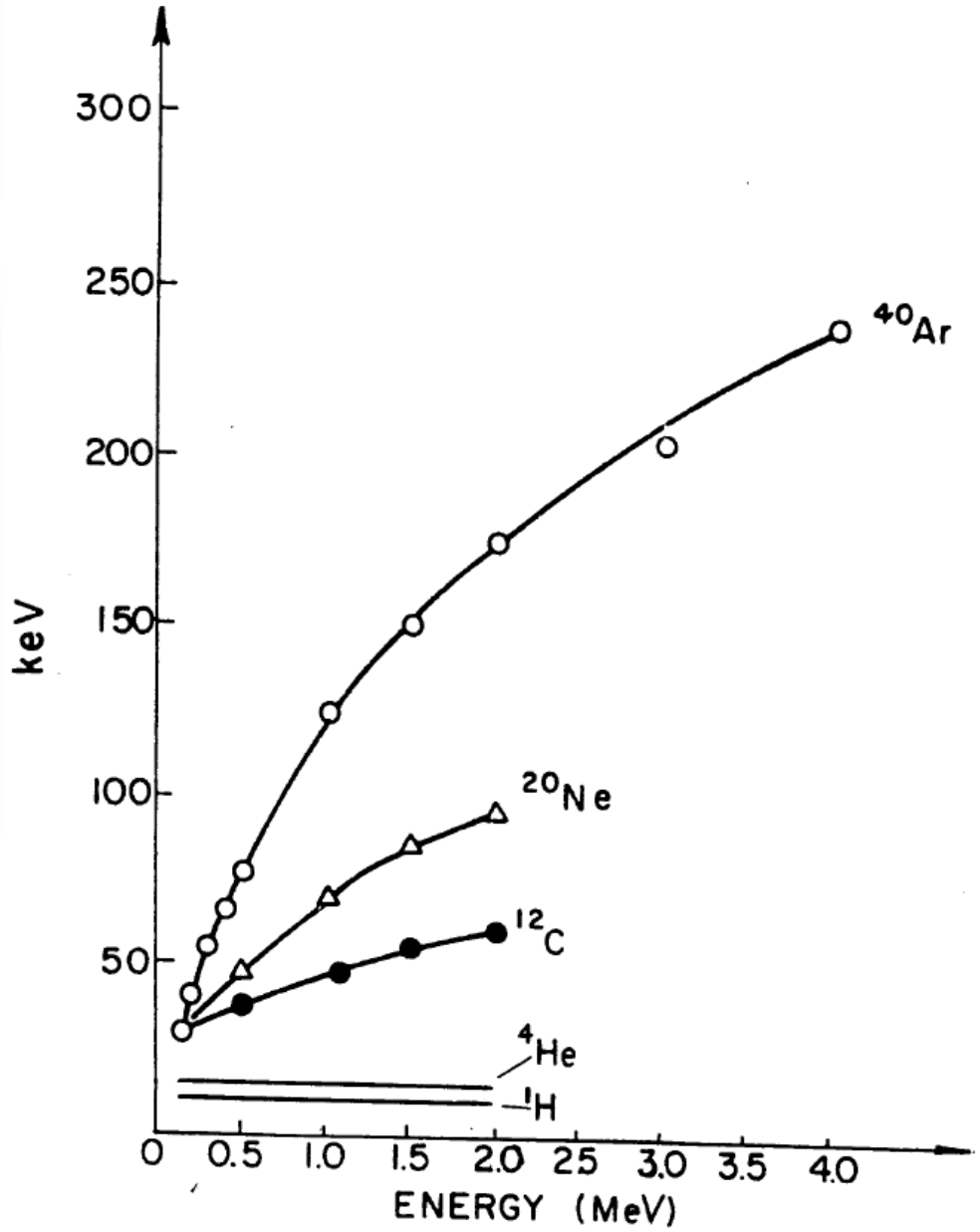

ELASTIC SCATTERING CROSS SECTION

For the COULOMB INTERACTION, a central force field, the differential scattering cross section of a target atom for scattering an incident particle through an angle θ into a differential solid angle $d\Omega$ centered about θ, in the laboratory frame of reference is given by:

$$\frac{d\sigma}{d\Omega} = \left(\frac{Z_1 Z_2 e^2}{2E\sin^2\theta}\right)^2 \frac{[\cos\theta + (1 - \mu^2\sin^2\theta)^{1/2}]^2}{(1 - \mu^2\sin^2\theta)^{1/2}}$$

$\mu = M_1/M_2$

E = energy of the projectile immediately before scattering

In backscattering spectrometry, the detector solid angle Ω is small (about 10^{-3} steradians) so that one defines an average differential scattering cross section:

$$\sigma(E,\theta) = (1/\Omega)\int_{\Omega}(d\sigma/d\Omega)d\Omega$$

and the scattering angle θ is well defined. It is then convenient[†] to introduce the *average differential scattering cross section* σ:

$$\sigma \equiv (1/\Omega) \int_{\Omega} (d\sigma/d\Omega)\, d\Omega. \tag{2.18}$$

For very small detector angles Ω, $\sigma \to d\sigma/d\Omega$. The average differential scattering cross section is the value ordinarily used in backscattering spectrometry. It is usually called *scattering cross section* in the literature. We follow this convention.

For the experimental condition given in Fig. 2.4, in which a uniform beam impinges at normal incidence on a uniform target that is larger than the area of the beam, the *total number of detected particles* A can be written from Eqs. (2.16) and (2.18) as

$$A = \sigma\Omega \cdot Q \cdot Nt. \tag{2.19}$$

$$\begin{pmatrix}\text{number of}\\ \text{detected particles}\end{pmatrix} = \sigma\Omega \cdot \begin{pmatrix}\text{total number of}\\ \text{incident particles}\end{pmatrix} \cdot \begin{pmatrix}\text{number of target}\\ \text{atoms per unit area}\end{pmatrix}.$$

This equation shows that when σ and Ω are known and the numbers of incident and detected particles are counted, the number of atoms per unit area in the target, Nt, can be determined. The ability of backscattering spectrometry to provide quantitative information on the number of atoms present per unit area of a sample stems from Eq. (2.19) and the fact that the average scattering cross section σ of the elements is known quite accurately.

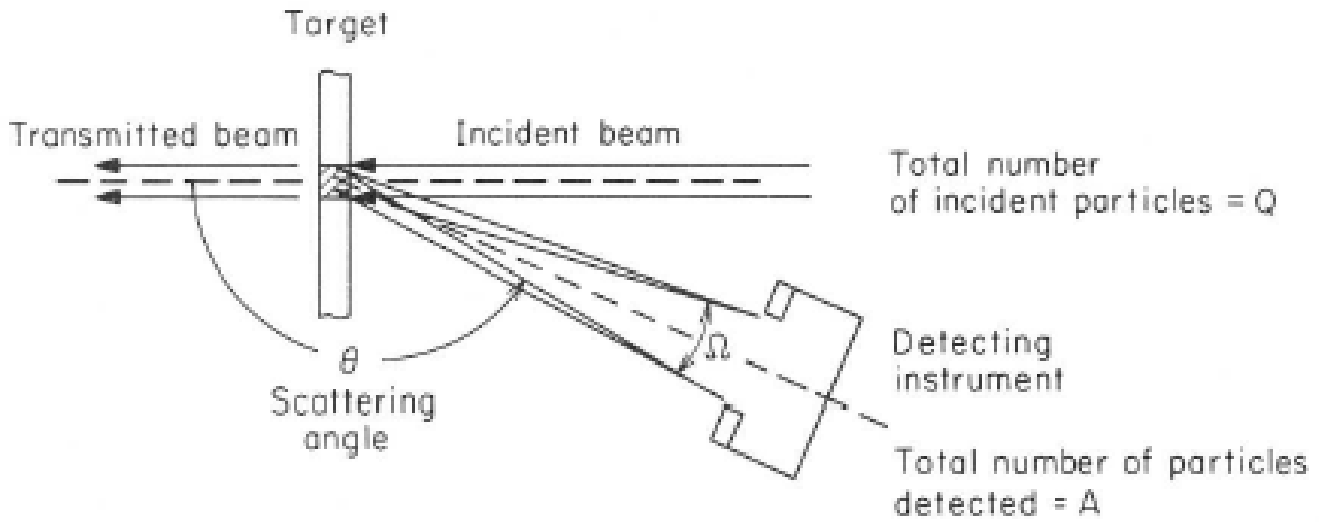

Fig. 2.4 Schematic layout of a backscattering experiment, showing a thin target, the transmitted portion of the beam, and the fraction of the backscattered beam that is intercepted and counted by the detector.

† In nuclear physics, the symbol σ is used to refer to the integral ("total") scattering cross section, called Σ in Eq. (2.17). The use of σ for the right-hand side of Eq. (2.18) is inconsistent with this older tradition, which would have required a symbol such as $\langle d\sigma/d\Omega \rangle$ instead. On the other hand, the newer (inconsistent) convention of Eq. (2.18) simplifies the writing of many equations to $\sigma\Omega$ rather than the clumsy $\langle d\sigma/d\Omega \rangle \Omega$.

TABLE X. Rutherford Scattering Cross Section of the Elements for 1 MeV ^{4}He

ELEMENT	AT. NO. (Z_2)	AVRG MASS (amu)	$d\sigma/d\Omega$ (in 10^{-24} cm^2/steradian)									
			179.5°	170°	160°	150°	140°	130°	120°	110°	100°	90°
BE	4	9.012	0.05344	0.05458	0.05817	0.06467	0.075	0.09069	0.1143	0.1503	0.2065	0.2972
B	5	10.81	0.09648	0.09837	0.1043	0.1149	0.1316	0.1569	0.1945	0.2514	0.3395	0.4814
C	6	12.01	0.1474	0.1502	0.1588	0.1744	0.1988	0.2354	0.29	0.3722	0.4992	0.7036
N	7	14.01	0.2142	0.218	0.2299	0.2513	0.2849	0.3351	0.4098	0.522	0.6952	0.9734
O	8	16	0.2915	0.2965	0.3122	0.3403	0.3844	0.4503	0.548	0.6947	0.921	1.285
F	9	19	0.3834	0.3898	0.4097	0.4455	0.5014	0.585	0.7089	0.8948	1.181	1.641
NE	10	20.18	0.4783	0.4862	0.5109	0.5551	0.6242	0.7275	0.8805	1.11	1.464	2.032
NA	11	22.99	0.5897	0.5993	0.6291	0.6827	0.7664	0.8915	1.077	1.355	1.783	2.47
MG	12	24.31	0.7064	0.7178	0.7534	0.8172	0.9169	1.066	1.286	1.617	2.126	2.944
AL	13	26.98	0.8378	0.8512	0.893	0.9678	1.085	1.26	1.518	1.907	2.505	3.465
SI	14	28.09	0.975	0.9905	1.039	1.126	1.262	1.464	1.765	2.215	2.908	4.022
P	15	30.97	1.127	1.145	1.201	1.301	1.457	1.689	2.034	2.551	3.347	4.625
S	16	32.06	1.286	1.306	1.369	1.483	1.66	1.925	2.317	2.905	3.811	5.265
CL	17	35.45	1.46	1.483	1.554	1.683	1.883	2.182	2.624	3.288	4.311	5.953
AR	18	39.95	1.646	1.671	1.752	1.895	2.12	2.455	2.951	3.696	4.842	6.683
K	19	39.1	1.832	1.861	1.95	2.11	2.36	2.734	3.287	4.116	5.394	7.444
CA	20	40.08	2.032	2.064	2.163	2.34	2.617	3.031	3.644	4.563	5.978	8.251
SC	21	44.96	2.249	2.285	2.394	2.589	2.895	3.351	4.027	5.04	6.601	9.106
TI	22	47.9	2.474	2.512	2.632	2.846	3.182	3.683	4.424	5.536	7.249	9.998
V	23	50.94	2.708	2.75	2.881	3.116	3.482	4.03	4.84	6.055	7.927	10.93
CR	24	52	2.95	2.996	3.138	3.394	3.793	4.389	5.271	6.594	8.633	11.91
MN	25	54.94	3.205	3.255	3.409	3.687	4.12	4.766	5.724	7.159	9.372	12.92
FE	26	55.85	3.468	3.521	3.689	3.989	4.457	5.157	6.192	7.745	10.14	13.98
CO	27	58.93	3.743	3.801	3.982	4.305	4.811	5.565	6.682	8.356	10.94	15.08
NI	28	58.71	4.026	4.088	4.282	4.63	5.173	5.984	7.185	8.986	11.76	16.21
CU	29	63.54	4.324	4.391	4.599	4.972	5.555	6.425	7.714	9.645	12.62	17.4
ZN	30	65.37	4.63	4.701	4.924	5.323	5.947	6.878	8.257	10.32	13.51	18.62
GA	31	69.72	4.948	5.024	5.262	5.688	6.355	7.349	8.821	11.03	14.43	19.89
GE	32	72.59	5.275	5.356	5.61	6.064	6.774	7.833	9.402	11.75	15.38	21.2
AS	33	74.92	5.612	5.698	5.968	6.451	7.206	8.333	10	12.5	16.36	22.54
SE	34	78.96	5.96	6.052	6.339	6.851	7.653	8.849	10.62	13.27	17.37	23.93
BR	35	79.91	6.317	6.414	6.718	7.261	8.11	9.378	11.25	14.07	18.4	25.36
KR	36	83.8	6.686	6.789	7.11	7.685	8.583	9.924	11.91	14.89	19.47	26.84
RB	37	85.47	7.064	7.173	7.512	8.119	9.068	10.48	12.58	15.73	20.57	28.35
SR	38	87.62	7.453	7.567	7.925	8.565	9.566	11.06	13.27	16.59	21.7	29.9
Y	39	88.91	7.851	7.972	8.348	9.023	10.08	11.65	13.98	17.47	22.86	31.5
ZR	40	91.22	8.26	8.388	8.784	9.494	10.6	12.26	14.71	18.38	24.05	33.14
NB	41	92.91	8.68	8.813	9.23	9.975	11.14	12.88	15.46	19.32	25.27	34.81
MO	42	95.94	9.11	9.251	9.687	10.47	11.69	13.52	16.22	20.27	26.52	36.54
TC	43	99	9.552	9.698	10.16	10.98	12.26	14.17	17	21.25	27.8	38.3
RU	44	101.1	10	10.16	10.64	11.49	12.84	14.84	17.81	22.25	29.1	40.1
RH	45	102.9	10.46	10.62	11.13	12.02	13.43	15.52	18.63	23.28	30.44	41.95
PD	46	106.4	10.94	11.1	11.63	12.57	14.03	16.22	19.46	24.32	31.81	43.83
AG	47	107.9	11.42	11.59	12.14	13.12	14.65	16.94	20.32	25.39	33.21	45.76

CD	48	112.4	11.91	12.09	12.66	13.69	15.28	17.67	21.2	26.49	34.64	47.73
IN	49	114.8	12.41	12.6	13.2	14.26	15.93	18.41	22.09	27.61	36.1	49.74
SN	50	118.7	12.93	13.13	13.74	14.85	16.59	19.17	23	28.75	37.59	51.8
SB	51	121.8	13.45	13.66	14.3	15.46	17.26	19.95	23.93	29.91	39.11	53.89
TE	52	127.6	13.99	14.2	14.87	16.07	17.94	20.74	24.89	31.1	40.67	56.03
I	53	126.9	14.53	14.75	15.45	16.69	18.64	21.55	25.85	32.3	42.25	58.2
XE	54	131.3	15.08	15.32	16.04	17.33	19.35	22.37	26.84	33.54	43.86	60.42
CS	55	132.9	15.65	15.89	16.64	17.98	20.08	23.21	27.84	34.79	45.5	62.68
BA	56	137.3	16.23	16.47	17.25	18.64	20.82	24.06	28.87	36.07	47.17	64.98
LA	57	138.9	16.81	17.07	17.87	19.31	21.57	24.93	29.91	37.37	48.87	67.32
CE	58	140.1	17.41	17.67	18.51	20	22.33	25.81	30.97	38.69	50.6	69.71
PR	59	140.9	18.01	18.29	19.15	20.69	23.11	26.71	32.04	40.04	52.36	72.13
ND	60	144.2	18.63	18.91	19.81	21.4	23.9	27.62	33.14	41.41	54.15	74.6
PM	61	147	19.26	19.55	20.47	22.12	24.7	28.55	34.25	42.8	55.97	77.11
SM	62	150.4	19.89	20.2	21.15	22.86	25.52	29.5	35.39	44.22	57.82	79.66
EU	63	152	20.54	20.86	21.84	23.6	26.35	30.46	36.54	45.66	59.7	82.25
GD	64	157.3	21.2	21.53	22.54	24.36	27.2	31.44	37.71	47.12	61.62	84.88
TB	65	158.9	21.87	22.2	23.25	25.13	28.05	32.43	38.9	48.6	63.56	87.56
DY	66	162.5	22.55	22.89	23.97	25.91	28.92	33.43	40.11	50.11	65.53	90.27
HO	67	164.9	23.24	23.59	24.71	26.7	29.81	34.45	41.33	51.64	67.53	93.03
ER	68	167.3	23.94	24.3	25.45	27.5	30.71	35.49	42.58	53.2	69.56	95.83
TM	69	168.9	24.65	25.03	26.2	28.32	31.62	36.54	43.84	54.77	71.62	98.67
YB	70	173	25.37	25.76	26.97	29.14	32.54	37.61	45.12	56.37	73.72	101.5
LU	71	175	26.1	26.5	27.75	29.98	33.48	38.69	46.42	58	75.84	104.5
HF	72	178.5	26.84	27.25	28.54	30.84	34.43	39.79	47.73	59.64	77.99	107.4
TA	73	181	27.59	28.01	29.33	31.7	35.39	40.91	49.07	61.31	80.17	110.4
W	74	183.9	28.35	28.79	30.14	32.57	36.37	42.04	50.43	63	82.38	113.5
RE	75	186.2	29.13	29.57	30.97	33.46	37.36	43.18	51.8	64.72	84.63	116.6
OS	76	190.2	29.91	30.37	31.8	34.36	38.36	44.34	53.19	66.46	86.9	119.7
IR	77	192.2	30.7	31.17	32.64	35.27	39.38	45.52	54.6	68.22	89.2	122.9
PT	78	195.1	31.5	31.99	33.49	36.19	40.41	46.71	56.03	70	91.53	126.1
AU	79	197	32.32	32.81	34.36	37.13	41.45	47.91	57.47	71.81	93.9	129.3
HG	80	200.6	33.14	33.65	35.24	38.08	42.51	49.13	58.94	73.64	96.29	132.6
TL	81	204.4	33.98	34.5	36.12	39.03	43.58	50.37	60.42	75.49	98.71	136
PB	82	207.2	34.82	35.36	37.02	40	44.67	51.62	61.92	77.37	101.2	139.4
BI	83	209	35.68	36.22	37.93	40.99	45.76	52.89	63.44	79.27	103.7	142.8
PO	84	210	36.54	37.1	38.85	41.98	46.87	54.17	64.98	81.19	106.2	146.2
AT	85	210	37.42	37.99	39.78	42.99	47.99	55.47	66.54	83.13	108.7	149.7
RN	86	222	38.31	38.89	40.73	44.01	49.13	56.79	68.12	85.1	111.3	153.3
FR	87	223	39.2	39.8	41.68	45.04	50.28	58.11	69.71	87.1	113.9	156.9
RA	88	226	40.11	40.72	42.64	46.08	51.45	59.46	71.32	89.11	116.5	160.5
AC	89	227	41.03	41.66	43.62	47.13	52.62	60.82	72.95	91.15	119.2	164.2
TH	90	232	41.95	42.6	44.6	48.2	53.81	62.19	74.6	93.21	121.9	167.9
PA	91	231	42.89	43.55	45.6	49.27	55.01	63.58	76.27	95.29	124.6	171.6
U	92	238	43.84	44.51	46.61	50.36	56.23	64.99	77.96	97.4	127.4	175.4

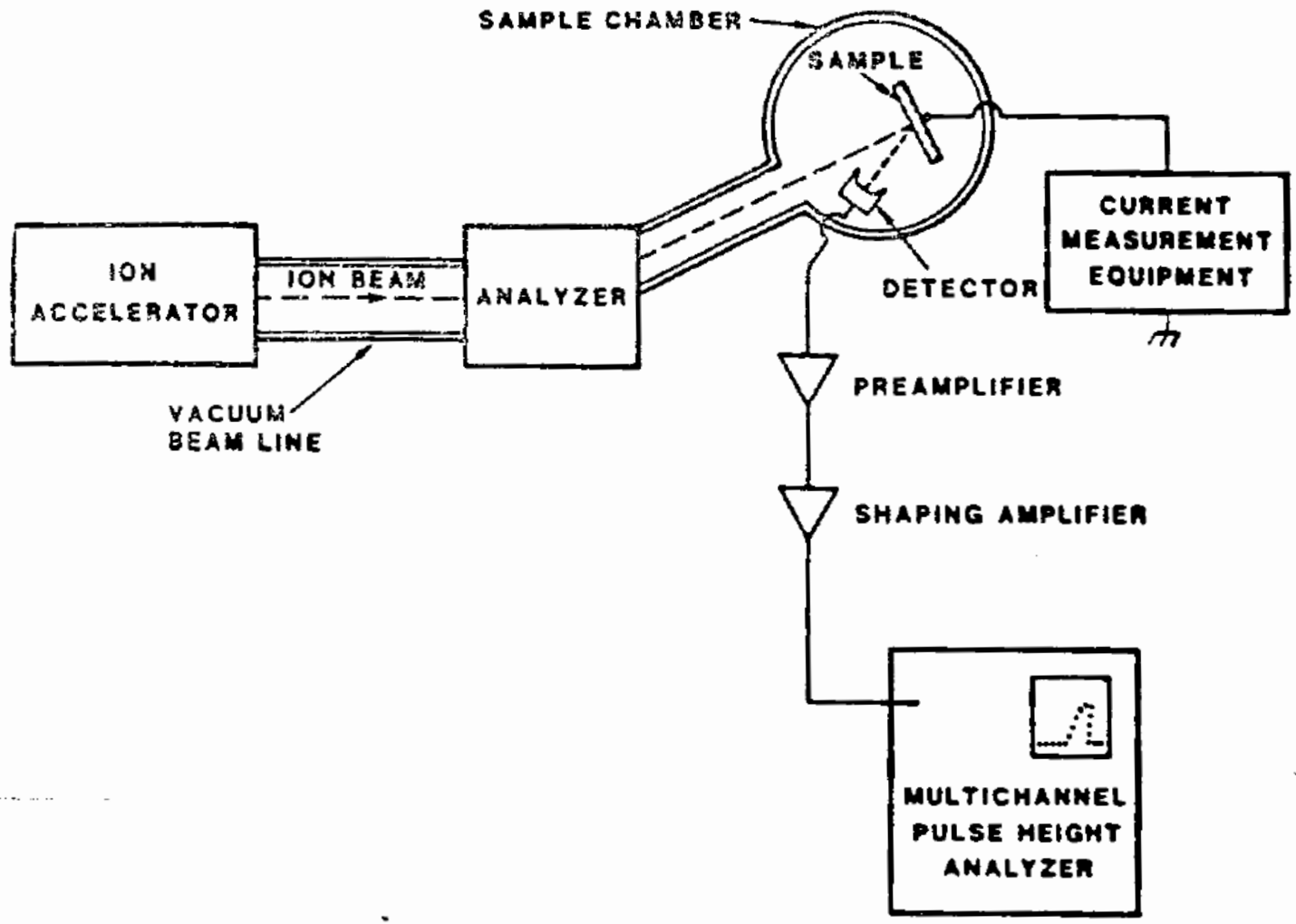

Simplified illustration of the equipment used for RBS.

For a thin target of thickness t with N atoms/cm^3, the YIELD, or the number of detected particles in a detector that subtend a solid angle Ω is:

$$Y = \sigma(E,\theta)\Omega Q N t$$

Q = total number of incident particles in the beam

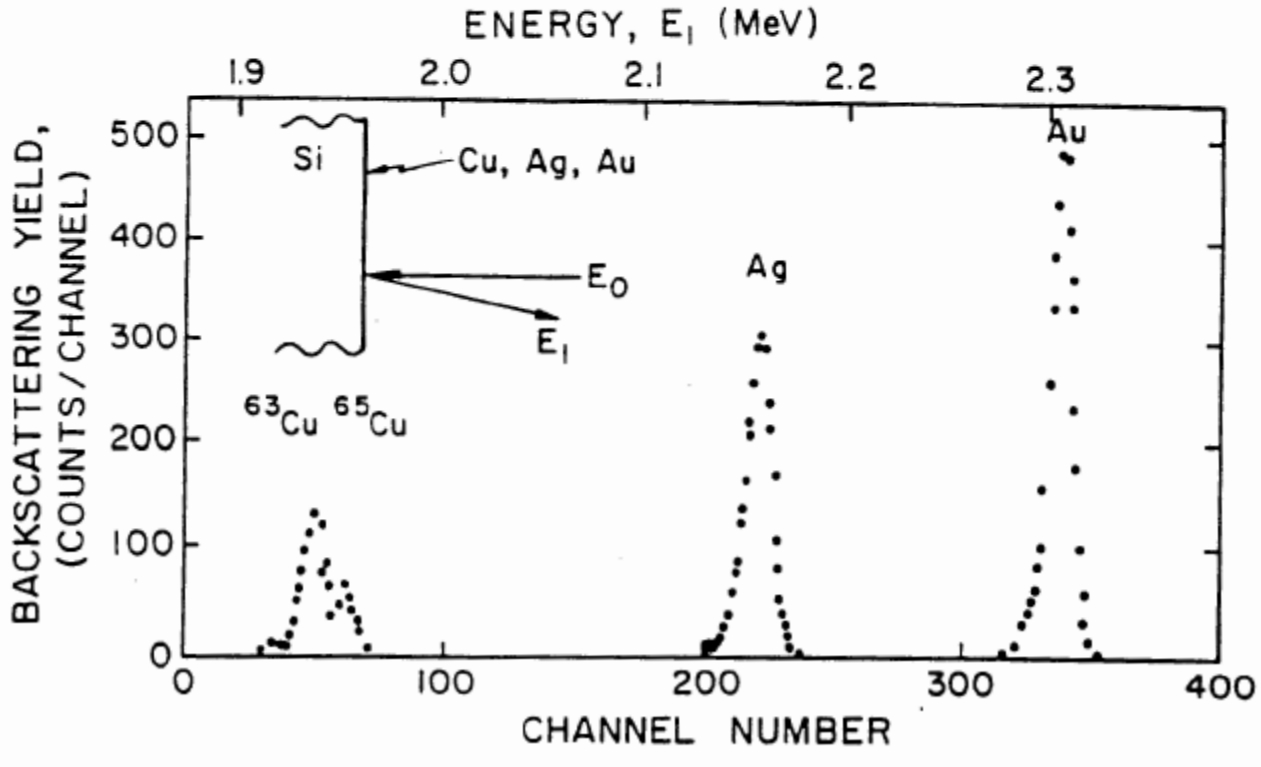

Peak areas scale with N and (in first approximation) with Z_2^2.

Absolute coverages of a heavy element on a light substrate can be detected down to a limit of about 10^{-3} monolayers.

ENERGY RESOLUTION:
DEPTH RESOLUTION

The energy resolution in a backscattering experiment is composed of two contributions:

- the "DETECTOR" RESOLUTION, ΔE_d
- the ENERGY STRAGGLING, ΔE_s

Assuming the two contributions are independent and satisfy Poisson's statistics, the total resolution, ΔE_1 (FWHM) is given by:

$$(\Delta E_1)^2 = (\Delta E_d)^2 + (\Delta E_s)^2$$

The ΔE_s term originates from the fact that an energetic particle moving through a medium loses energy via many individual encounters. Such a discrete process is subject to statistical fluctuations. As a result the energy loss ΔE is subject to fluctuations. The phenomenon is called energy straggling. For MeV He or H ions a good approximation for energy straggling is given by the Bohr's formula:

$$\Omega^2 = 4\pi(Z_1 e^2)^2 Z_2 N t$$

Clearly, for scattering at the surface we have $\Delta E_s = 0$

2.6 ENERGY STRAGGLING

An energetic particle that moves through a medium loses energy via many individual encounters. Such a quantized process is subject to statistical fluctuations. As a result, identical energetic particles, which all have the same initial velocity, do not have exactly the same energy after passing through a thickness Δx of a homogeneous medium. The energy loss ΔE is subject to fluctuations. The phenomenon, sketched in Fig. 2.10, is called *energy straggling*. Energy straggling places a finite limit for the precision with which energy losses, and hence depths can be resolved by backscattering spectrometry. The ability to identify masses is also impaired, except for atoms located at the surface of the target. The reason is that the beam energy E before a collision with a specific mass M_2 at some depth within the target is no more monoenergetic, even if it was so initially, so that the ratio E_1/E_0, and hence the identification of M_2, become uncertain as well. For these reasons, it is important to have quantitative information on the magnitude of energy straggling for any given combination of energy, target material, target thickness, and projectile.

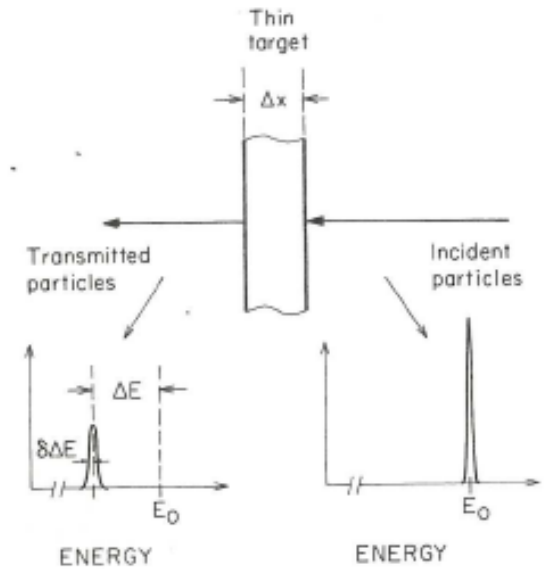

Fig. 2.10 A monoenergetic beam of energy E_0 loses energy ΔE in traversing a thin film of thickness Δx. Simultaneously, energy straggling broadens the energy profile.

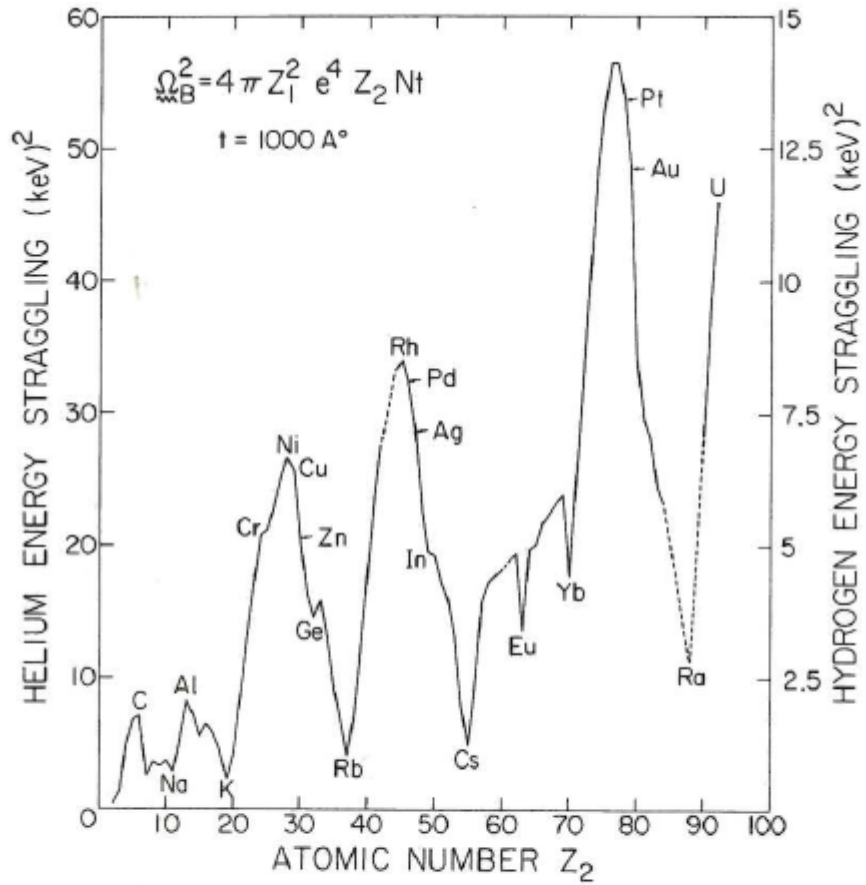

Fig. 2.11 The value of the variance $\Omega_B{}^2 = 4\pi Z_1{}^2 e^4 Z_2 Nt$ for $t = 1000$ Å for energy straggling according to the classical model of Bohr for electronic energy loss versus the atomic number of the target atom. The pronounced structure reflects the difference in the atomic density of the elements.

2.7 LINEAR ADDITIVITY OF ENERGY STRAGGLING

Experimental data on energy straggling below 2 MeV for ^{1}H and ^{4}He in solid elemental targets are few. For solid compound targets, no experimental data exist at all. The need for information is obvious. Until such results become available, statements on energy straggling in solid compounds must necessarily be conjectural.

The most obvious suggestion as to how energy straggling behaves in a compound or a mixture A_mC_n proceeds as follows (Chu, 1976). Let N_A and N_C be the volume densities of the individual elements A and C, and let $N^{A_mC_n}$ be the volume density of compositional units A_mC_n in the mixture or compound. Assume that for a thickness t, the energy straggling in elements A and C individually is [Eq. (2.56)]:

$$(\Omega_B^{\ A})^2 = 4\pi(Z_1e^2)^2 N_A Z_A t, \tag{2.65}$$

$$(\Omega_B^{\ C})^2 = 4\pi(Z_1e^2)^2 N_C Z_C t. \tag{2.66}$$

This means that $(\Omega_B^{\ A})^2/N_A Z_A t = (\Omega_B^{\ C})^2/N_C Z_C t = 4\pi(Z_1e^2)^2$ is independent of the target, the ratio being simply the square of the energy variance per electron in a unit area of the target with thickness t. An extension of Bohr's model to a compound target then predicts that this quantity should apply independently of the composition of the target, or

$$\frac{(\Omega_B^{A_mC_n})^2}{\begin{pmatrix}\text{number of electrons per unit}\\ \text{area of the target of thickness } t\end{pmatrix}} = 4\pi(Z_1e^2)^2, \tag{2.67}$$

and therefore

$$(\Omega_B^{A_mC_n})^2 = 4\pi(Z_1e^2)^2 N^{A_mC_n}(mZ_A + nZ_C)t. \tag{2.68}$$

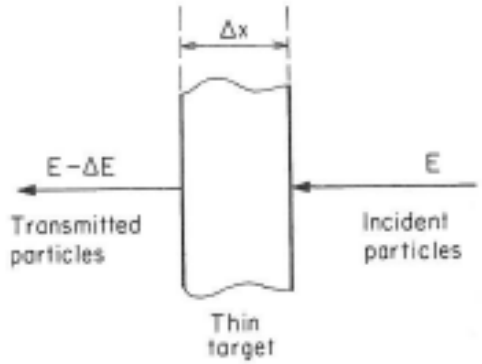

Fig. 2.6 Schematic of a transmission experiment to measure the $\Delta E/\Delta x$ loss of a swift particle in a dense medium.

the target, it slows down and its kinetic energy $E = \frac{1}{2}M_1 v^2$ decreases. The amount of energy ΔE lost per distance Δx traversed depends on the identity of the projectile, on the density and composition of the target, and on the velocity itself. The simplest experiment that can be conceived to determine this energy loss is to take a very thin target of thickness Δx and of known composition. A beam of monoenergetic particles is directed at this target (see Fig. 2.6). The energy difference ΔE of the particles before and after transmission through the target is measured. The *energy loss* per unit length, also called sometimes the *specific energy loss*, and frequently abbreviated *dE/dx loss*, at the energy E of the incident beam is then defined as

$$\lim_{\Delta x \to 0} \Delta E/\Delta x \equiv \frac{dE}{dx}(E) \tag{2.25}$$

for that particular particle and energy in that medium. Note that this expression gives an energy loss that is a positive quantity.

http://srim.org/

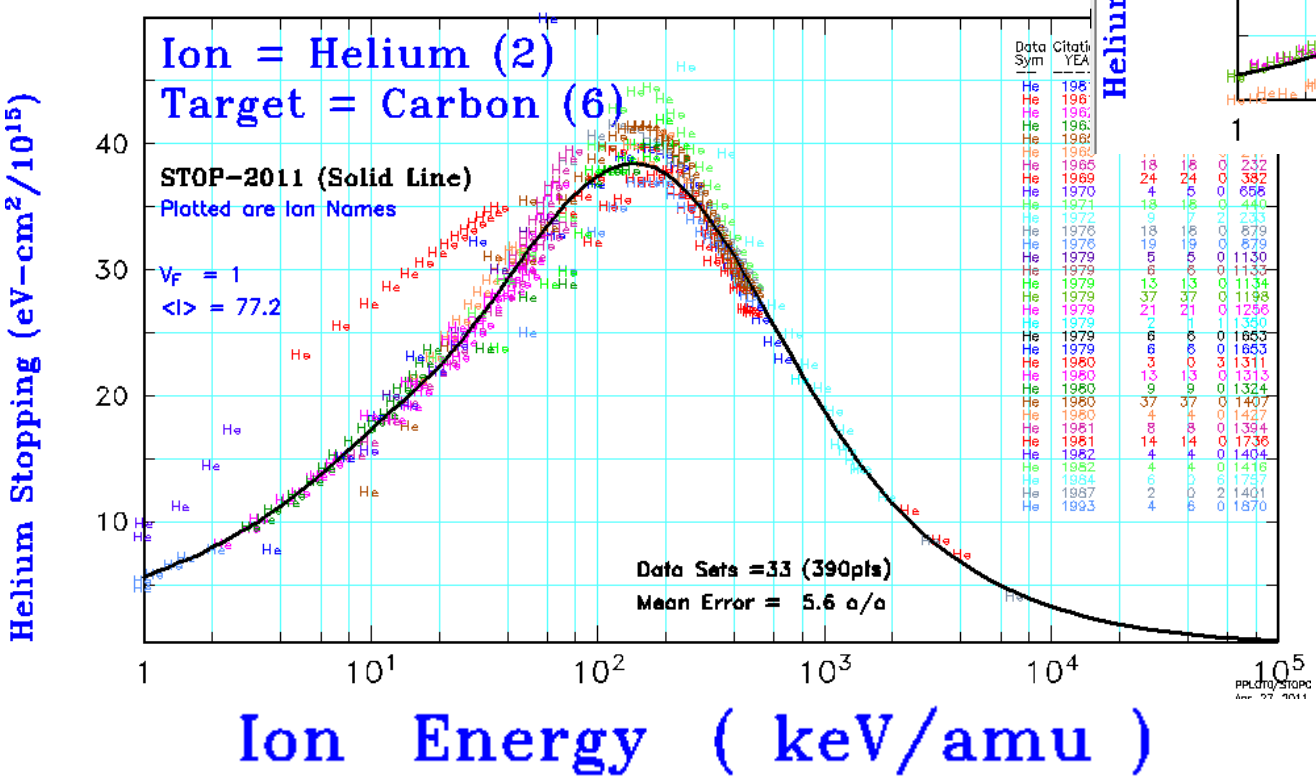

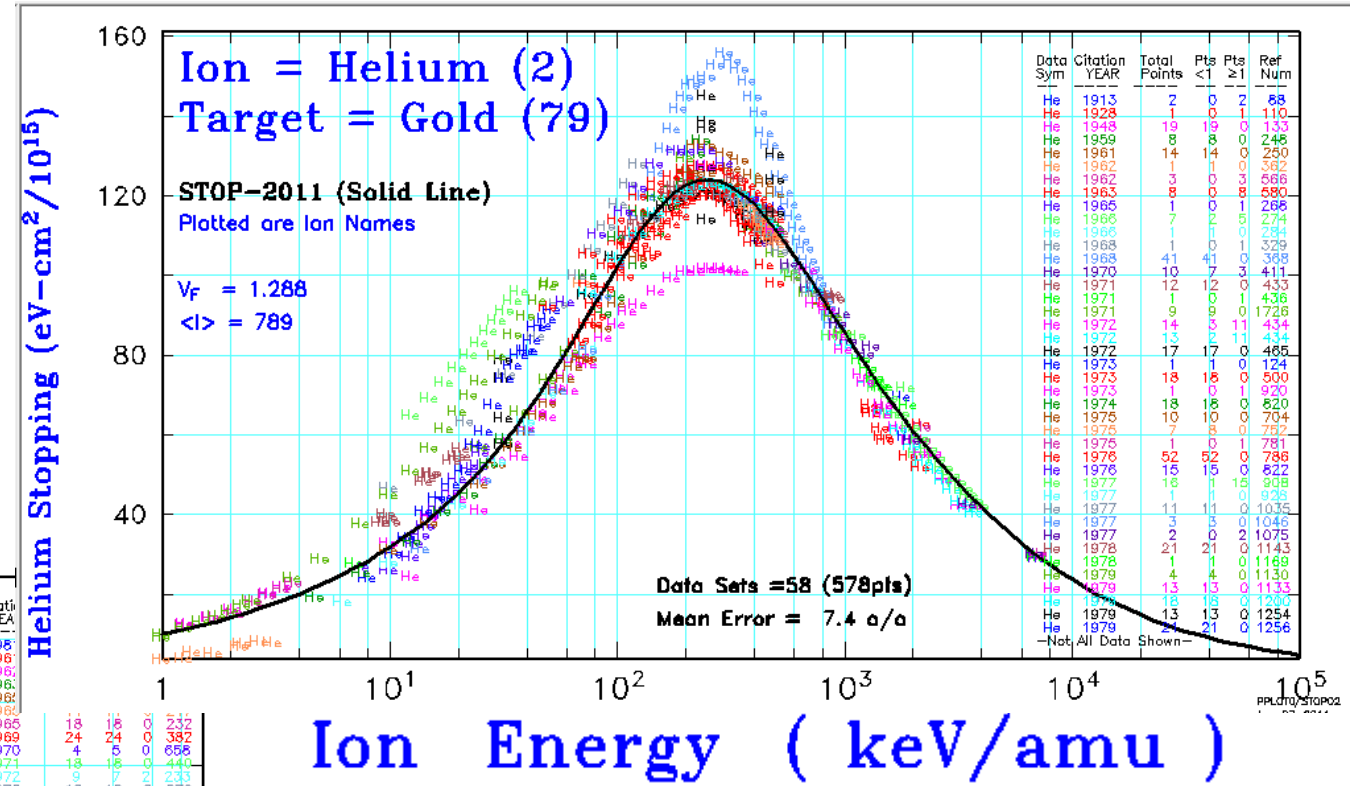

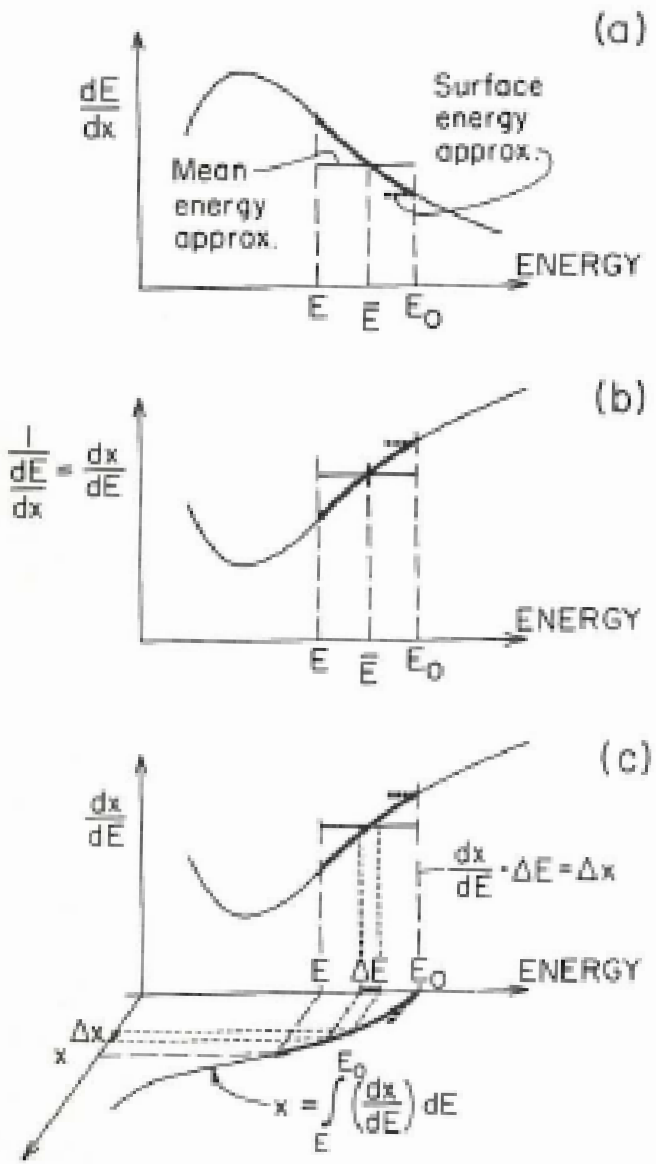

$$dx = \frac{dx}{dE}(E) \cdot dE,$$

$$x = \int_E^{E_0} (dx/dE)\, dE = \int_E^{E_0} (dE/dx)^{-1}\, dE.$$

Fig. 2.7 (a) Typical dependence of dE/dx as a function of the kinetic energy E of the projectile. To obtain the depth of penetration x at which the particle energy has been reduced from E_0 to $E < E_0$, one takes the reciprocal of dE/dx, as shown in (b), and integrates this function from E to E_0, as represented in (c). In the surface energy approximation, dE/dx is replaced by its value at E_0 (heavy dashed line). In the mean energy approximation, the constant value of dE/dx is chosen at the mean energy $\bar{E} = \frac{1}{2}(E + E_0)$.

$$H_0 = \sigma(E_0)\Omega Q\mathscr{E}/[\varepsilon_0]\cos\theta_1. \tag{3.38}$$

This equation states that the height of the energy spectrum at the surface is directly proportional to

(i) Q, the total number of incident projectiles bombarding the sample;
(ii) $\sigma(E_0)$, the average differential scattering cross section between the projectile and the sample evaluated at the incident energy E_0;
(iii) Ω, the solid angle spanned by the detector aperture;
(iv) $\mathscr{E}$, the energy width of a channel, which is determined by the electronic setting of the detecting system; and
(v) $([\varepsilon_0]\cos\theta_1)^{-1}$, the inverse of the stopping cross section factor evaluated at the surface for a given scattering geometry multiplied by the cosine of the angle of incidence of the beam against the sample normal.

The direct proportionality of H_0 to Q, σ, Ω, and $\mathscr{E}$ is physically evident. The inverse proportionality of H_0 to $[\varepsilon_0]\cos\theta_1$ can be understood by considering the energy that particles lose on their inward and outward paths through the surface layer. Consider first the case of normal incidence. If the stopping cross section is high, then so is the stopping cross section factor $[\varepsilon_0]$.

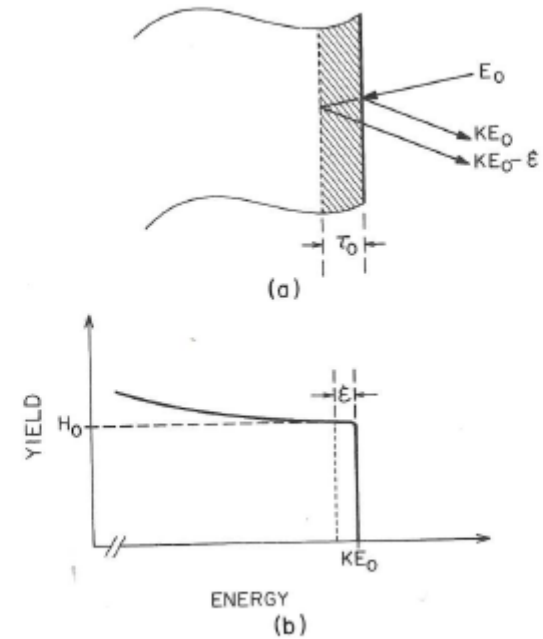

Fig. 3.12 Schematic of the backscattering process in the surface region of a sample consisting of a monoisotopic element (a) and the resulting spectrum (b).

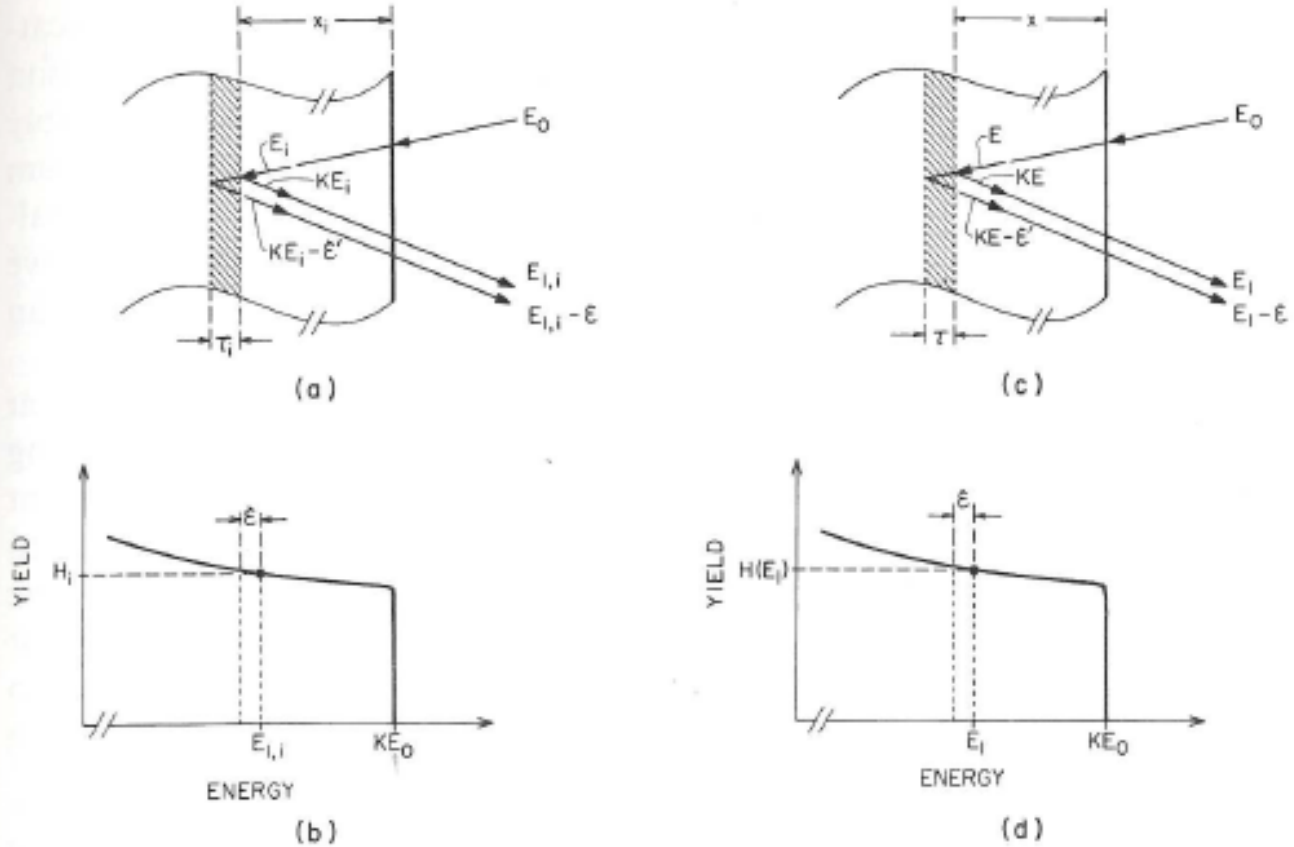

Fig. 3.13 Schematics of and nomenclature for (a) the backscattering process at depth x_i within a monoisotopic sample in the language of discrete functions, and (b) the resulting spectrum. (c) and (d) give the corresponding schematics and nomenclature in the language of continuous functions.

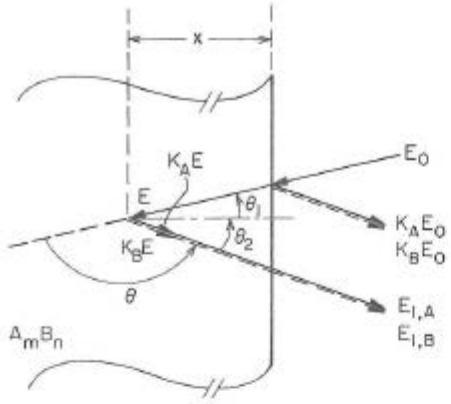

Fig. 3.15 Symbols used in the description of backscattering events in a compound sample composed of a homogeneous mixture of two monoisotopic elements A and B.

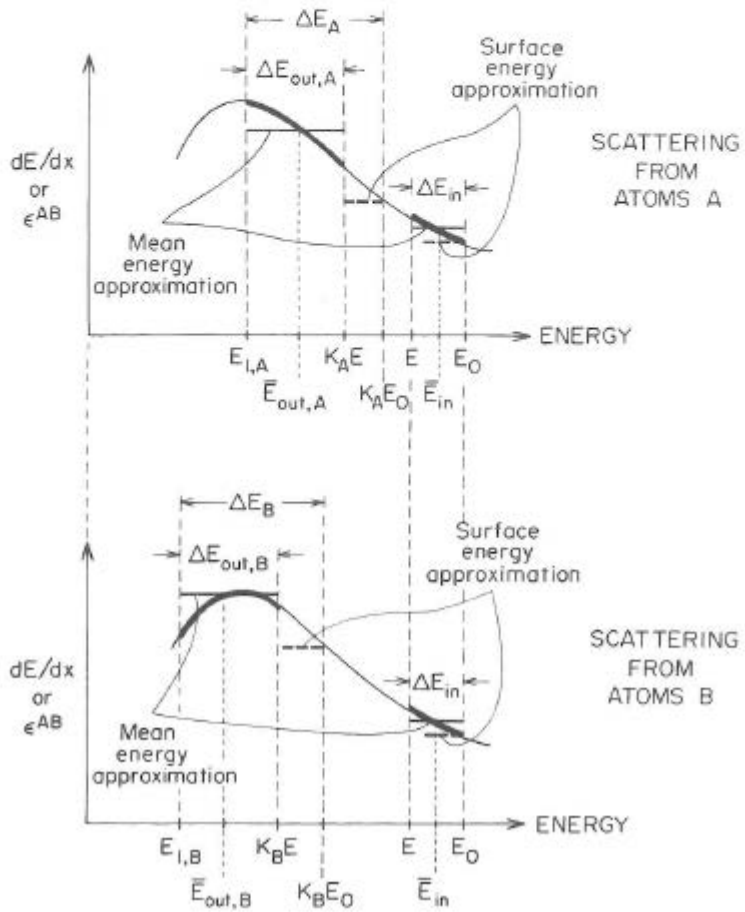

Fig. 3.16 Graphical representations of the energy loss of particles along their inward and outward paths (heavy lines) through a sample composed of a homogeneous mixture of two monoisotopic elements A and B. The light line is the functional form of dE/dx versus E. Since $dE/dx = N^{AB}\varepsilon^{AB}$, the same plots apply to ε^{AB} versus E as well. Particles scattered at the two elements cover different energy ranges along their outward paths. The top of the figure applies for scattering by the heavy atom A; the bottom of the figure is for scattering by the atom B which is lighter than A. (Compare this with the corresponding parts of Fig. 3.7 for a monoisotopic sample.)

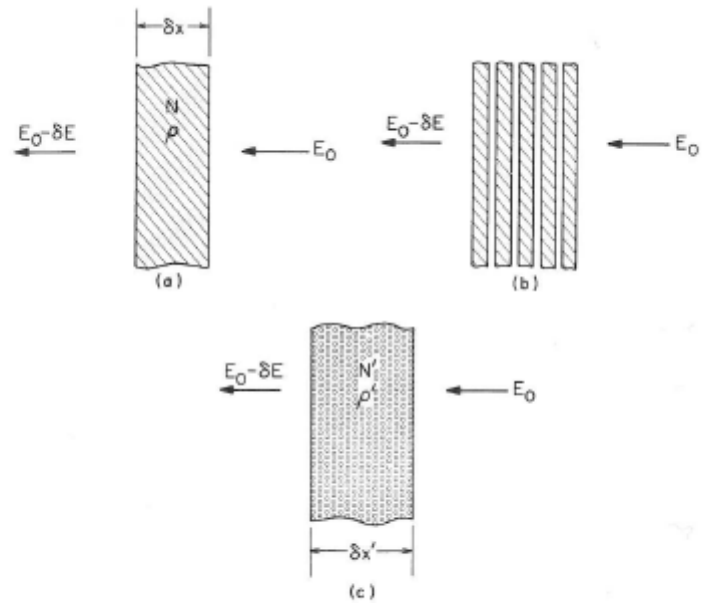

Fig. 3.20 Three different samples of the same material but different overall density all of which generate the same backscattering spectrum.

http://srim.org/